MATHEMATICAL MODELING OF GAS DYNAMICS AND HEAT EXCHANGE IN ROTATING FURNACE

V. A. Arutyunov and A. V. Povitskii

UDC 536.24:621.78.04

This paper describes a mathematical model of the turbulent diffusion flame and complex heat transfer in a rotating furnace. A numerical study is made of the dependence of flame configuration on the air delivery factor. The influence on flame length of the momentum flux density ratio for the oxidizing agent and fuel gas is investigated. The relationship between flame length and the proportion of the fuel gas delivered through the annular passage of an adjustable two-passage burner is established. The temperature distributions over the length of the furnace are calculated for various flame configurations.

The rotating furnace (RF) is a piece of continuous-operation industrial equipment whose working space has the form of a hollow cylinder. As a consequence of the small degree of inclination and the rotation of the furnace, the granular material being processed is displaced while being warmed by the heat released when fuel is burned in the working space. RFs are widely used in ferrous and nonferrous metallurgy and in the building-materials industry [1].

One important approach to improving furnace operating efficiency is upgrading of burner design. Conflicting requirements are imposed on the flame in annealing RFs: it has to be sufficiently long to provide the requisite extent for the annealing zone and prevent overheating of the material and simultaneously be sufficiently inflexible and hot to assure that the material is heated to the annealing temperature. The fuel burning rate must be controlled in order to reduce the amount of overheated material that adheres to the lining.

Flame length is generally determined indirectly, from the RF outside surface temperature, because of the complexity of measuring the temperature, concentration, and gas dynamic fields in the working space [2].

The development of numerical methods for solving gas dynamic problems allows us to devise a mathematical model for a diffusion flame and to calculate its characteristics.

The turbulent motion of gases is described by the Reynolds equations. Numerical solution of these three-dimensional problems for flows accompanied by combustion is possible [3] but requires extremely large amounts of computer time.

Axially symmetric burners are generally employed in rotating furnaces. Temperature measurements in the working space of an RF [4] showed that the flame occupied a symmetric position in it. Some breakdown of this symmetry occurs only in the tail of the flame, because of the segmental disposition of the material bed. The gas dynamics of such a flame are consequently described by two-dimensional equations in cylindrical coordinates (x, r):

$$\frac{\partial}{\partial x}\left(\Gamma_F\frac{\partial F}{\partial x}-\rho uF\right)+\frac{1}{r}\frac{\partial}{\partial r}\left(\Gamma_{Fr}\frac{\partial F}{\partial r}-rv\rho F\right)+S_F=0, \tag{1}$$

where F = u, v, K, ε, C_g', g.

Replacement of elliptic equations (1) by parabolic equations (of the boundary layer equation type) is valid only for calculating the flows in large-diameter furnaces having burners with sharp-edged nozzle rims, where the recirculation zones are small in size and the velocity in them is close to zero. In this case, the terms describing the transverse

Moscow Institute of Steel and Alloys. Translated from Inzhenerno-fizicheskii Zhurnal, Vol. 61, No. 3, pp. 406-413, September, 1991. Original article submitted December 26, 1989.

 0022-0841/91/6103-1098$12.50

convective and longitudinal gradient-transport components are neglected in Eq. (1).

Writing the equations of motion in the variables u–v–p rather than teh variables ω–ψ (vorticity versus flow function) permits use of the pressure field to determine the velocity and flow rate of the air entering the furnace by gravity flow through the cooler, as a consequence of injection by the high-speed gas jet.

The turbulence model of [5] is used to determine the coefficient of turbulent transport; it includes Eq. (1) for K and ε and the ratio

$$\Gamma_F = \frac{1}{\mathrm{Pr}_F}\left(C_\mu \rho \frac{K^2}{\varepsilon} + \mu\right).$$

We have made the following assumptions: the combustion reaction is single-stage and irreversible, and the combustion process takes place in the diffusion region. The latter fact is due to the use of non-premixing burners and the high combustion product temperature. Given these assumptions, it is best to utilize the adjusted fuel concentration C_g' as the main variable [6]:

$$C_g' = C_g + \frac{1}{\Omega + 1} C_{pr}.$$

The value of C_g' is employed to calculate the unique reagent concentrations at each point.

When computing the temperature fields, it is generally necessary to have the model include transport equations (1) for the enthalpy of deceleration. However, since we are assuming flow to be adiabatic, it is not necessary to solve Eq. (1) for the enthalpy, and the temperature should be determined from the algebraic equation expressing the heat balance for each point:

$$\begin{aligned}(c_{p_g} C_g + c_{p_{ox}} C_{ox} + c_{p_{pr}} C_{pr})(T - 273) = c_{p_{g0}} C_g (T_g - 273) + \\ + c_{p_{ox0}} C_{ox}(T_{ox} - 273) + c_{p_{pr_0}} C_{pr}(T_f - 273),\end{aligned} \tag{2}$$

where T is the unknown temperature at a given point, while the index 0 indicates that c_p has been taken for temperatures T_g, T_{ox}, and T_f respectively.

The applicability of this simplified approach to calculations for RF flames was investigated in [7]; it was found that, although relation (2) introduces an error into the temperature determinations, it has little influence on the computed flame configuration.

The theoretical combustion temperature is calculated with the partial product dissociation taken into account by utilizing equations that relate the equilibrium constants of the CO_2 and H_2O dissociation reactions to the degrees of dissociation, the heat balance relation at the combustion front, and the Van't Hoff formulas expressing the dependence of the equilibrium constants on temperature:

$$K_1 = \left(\frac{1 - \alpha_{CO_2}}{\alpha_{CO_2}}\right)^2 \frac{1 + 0{,}5\,(\alpha_{CO_2} C_{CO_2} + \alpha_{H_2O} C_{H_2O})}{0{,}5\,(\alpha_{CO_2} C_{CO_2} + \alpha_{H_2O} C_{H_2O})}, \tag{3}$$

$$\alpha_{H_2O} = \frac{\alpha_{CO_2}}{\sqrt{\frac{K_2}{K_1}(1 - \alpha_{CO_2}) + \alpha_{CO_2}}}, \tag{4}$$

$$\begin{aligned}c_{p_{g0}} C_g (T_g - 273) + c_{p_{ox0}} C_{ox}(T_{ox} - 273) + Q_i^f - \\ - Q_{CO_2}^d \alpha_{CO_2} C_{CO_2} - Q_{H_2O}^d \alpha_{H_2O} C_{H_2O} = c_{p_{pr0}}(T_{cr} - 273),\end{aligned} \tag{5}$$

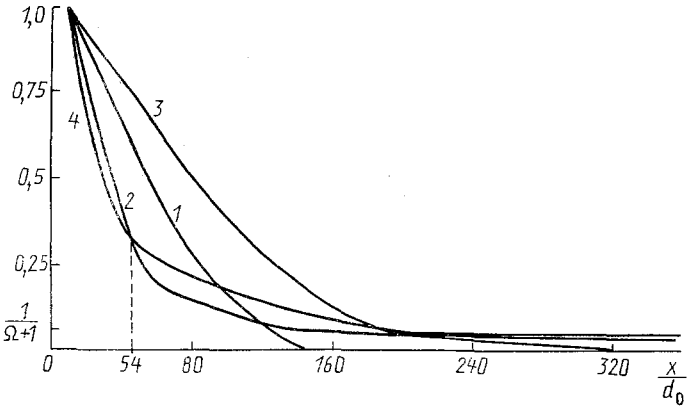

Fig. 1. Reduced concentration and fuel depletion as functions of distance to nozzle exit section with different values for association parameter. 1) Fuel depletion; 2) reduced concentration for $I_{sd} = 0.39$; 3, 4) the same for $I_{sd} = 10^{-4}$.

$$\lg K_1 = \frac{29250}{T} - 2{,}5 \lg T - 1{,}24, \tag{6}$$

$$\lg \frac{K_2}{K_1} = -\frac{2125}{T} + 1{,}96. \tag{7}$$

Equation (3) is solved for α_{CO_2} by bisection on the interval [0; 1]; the front temperature is determined from Eq. (5), in combination with (4), (6), and (7) in each iteration. The resultant combustion product composition and front temperature are utilized in Eq. (2).

If we take into account the turbulent fluctuations in the local concentration, the time-averaged density is defined by the expression

$$\rho = \int_0^1 \rho(C)\, q(C)\, dC,$$

where $\rho(C)$ is the dependence of the density on the reduced concentration and is determined from the equation of state; $q(C)$ is the probability that the reduced concentration will lie in the interval $[C - dC/2;\ C + dC/2]$. The probability density $q(C)$ is utilized in the model in the form of the sum of Dirac δ-functions that include the mean square fluctuation g as a parameter; it was suggested in [8] that the latter be determined by using a transfer equation of the type of (1).

Our calculations showed that assuming a diffuse front lowers the temperature within it by 150-200°C, affects flame configuration, and improves computational stability.

Boundary conditions are imposed at the furnace inlet on the basis of the specified fuel delivery rate, air passage pressure loss, nozzle geometry, and initial turbulence conditions. The turbulent energy at near-wall points is determined by the patterns in the logarithmic region of the boundary layer [9]. The derivatives with respect to r and x are accordingly zero at the symmetry axis and in the exit cross section.

Equations of the type of (1) are solved by the finite difference method. The form of the finite-difference analog depends on the local net Peclet number [10]. A central-difference scheme is employed for all terms when $|Pe| \leq 2$; a "counterflow" scheme is used to approximate the convective terms when $|Pe| > 2$, and gradient transport is neglected. Three nets are utilized in the numerical calculations: one for the axial velocity (x_u, r), one for the radial velocity (x, r_v), and one for the other variables (x, r). The collections of node coordinates x_u and r_v are specified in constructing the nets, while the coordinates x and r are calculated from the formulas:

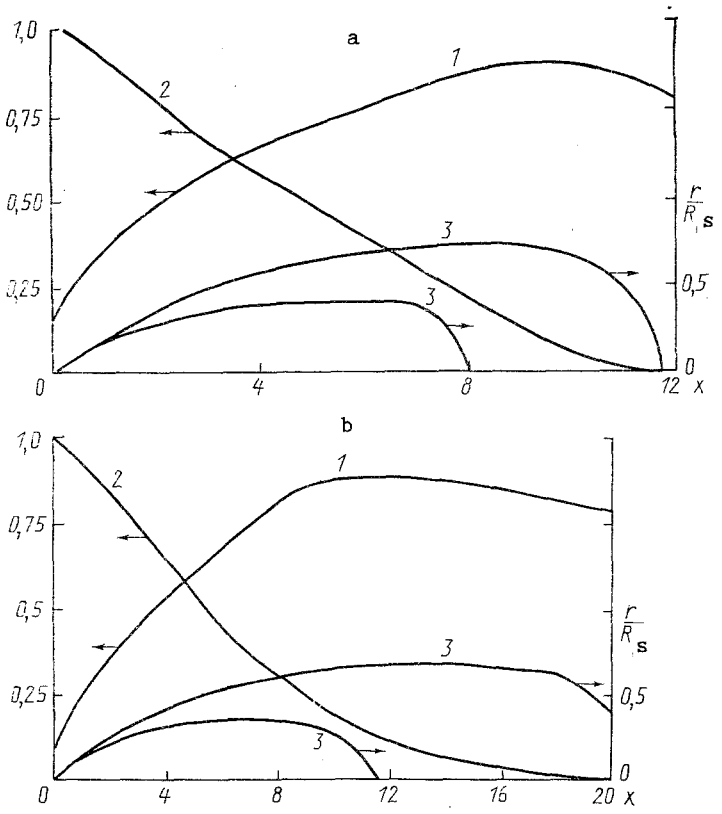

Fig. 2. Temperature at axis and fuel depletion for two-passage burner with controllable flame length. a) Minimum flame length; b) maximum flame length; 1) normed axial temperature (T/T_f); 2) fuel depletion; 3) outer and inner flame front boundaries (r/R_s). x is in m.

$$x(1) = x_u(1);\ x(j) = 0{,}5\,(x_u(j-1) + x_u(j));$$
$$j = 2,\ldots,\ M-1;\ x(M) = x_u(M-1);$$
$$r(1) = r_v(1);\ r(i) = 0{,}5\,(r_v(i-1) + r_v(i));$$
$$i = 2,\ldots,\ N-1;\ r(N) = r_v(N-1),$$

where M is the number of nodes along the x-axis and N is the number of nodes along the r-axis.

A coordinate r_v corresponds to each nozzle boundary, i.e., to each discontinuity in the boundary conditions. The r_v lines cluster near the axis and the x_u lines near the nozzles, and the distance between coordinates x_u increases with the distance from a nozzle by a geometric progression with common ratios ranging from 1.001 to 1.01. The net spacing is thus less in regions with a large velocity gradient than in regions with a small gradient.

The SIMPLE method [10] is used to determine the pressure field. It essentially consists of determining a pressure field correction in each iteration, employing the continuity equation with the velocity replaced by its expression in terms of the pressure correction.

When the finite difference analog of Eq. (1) is solved for some variable, the coefficients depending on other variables are assumed to be constant, which necessitates multiple iterations of the entire system.

The Gauss–Seidel method is used to solve each equation, since it makes no sense to obtain an exact solution in each iteration when the values of the "frozen" coefficients are inexact. The coefficients of relaxation from below amount from 0.5 to 0.75.

Convergence is assumed to be attained if the maximum cross-sectional mass flux error does not exceed 1%. Calculations made for a 20 × 80 net in an ES-1061 computer required $1.7 \cdot 10^{-3}$ sec per net node per iteration, and from 500 to 1000 iterations were needed for convergence.

A flame organized in the same manner as in an RF was investigated in [11]: the fuel gas was delivered through a central nozzle and the air through an enclosing annular passage. The combustion chamber was cylindrical. We compared our calculated flame configuration and momentum flux density distribution results with the experimental data of [11] and found the agreement to be satisfactory.

Calculations were made for the flame from a single-passage burner in a rotating furnace with the following parameters: a nozzle radius of 25 mm, a working space radius of 1500 mm, a stoichiometric ratio of 17.2 kg/kg, a gas temperature of 300 K, gas outflow velocity of 400 m/sec, an air temperature of 500 K, and all air delivered to the furnace through a cooler (so-called secondary air). The air delivery factor α was varied from 1.01 to 1.2. When $\alpha = 1.01$, the lack of air caused the flame to remain open along the axis for a distance of 20 m from the nozzle opening; flame length was 17 m $(340d_0)$ when $\alpha = 1.1$ and 12.5 m $(250d_0)$ when $\alpha = 1.2$. The combustion graphs were identical over the first 10 m, i.e., the air delivery rate had a significant effect on the flame configuration only in the tail. The outer combustion front boundary reached $0.6R_s$.

When the secondary air delivery to the furance was inadequate, additional primary air or oxygen was supplied through the annular passage surrounding the fuel gas delivery passage.

The question of the influence exerted by the momentum flux density ratio I_{sd} for the oxidizing agent and fuel on flame length has not been conclusively resolved. Thus, it was established in [11] that flame length increases when I_{sd} is lowered from 2.2 to 0.4, and it was shown in [1] that maximum flame length is attained when I_{sd} is close to 1. Calculations were made for flames produced at different air velocities with coke-oven ($\Omega = 1.69$ kg/kg) and natural gas. The coke gas delivery rate was chosen so as to five identical furnace thermal power levels for both types of fuel. Half of all the air was forced through the annular passage, so that $I_{sd} = 0.39$. Figure 1 shows graphs for the reduced concentration and fuel depletion z along the furnace axis for the case in question and for 100% secondary air ($I_{sd} \approx 10^{-4}$). The total air delivery factor was the same for both cases. The length of the natural gas flame with 50% forced air delivery was 7.5 m $(150d_0)$. The reduced concentration on the axis at a distance of less than 2.7 m $(54d_0)$ from the nozzle opening was greater for 50% forced air delivery, but the situation was reversed at greater distances.

The length of the coke gas flame was $30d_0$ for forced air delivery and $40d_0$ for free delivery. The reduced concentration on the axis was greater for free air delivery, regardless of the distance from the nozzle exit section. The length of the potential flame core was $2.4d_0$ for force delivery and $8.2d_0$ for free delivery. This result contradicted data indicating that the potential core length for an isothermal jet increases as I_{sd} is raised from 0 to 1, which can be attributed to the substantial influence of nonisothermality on effective viscosity. Qualitative analysis of conservative figures reveals two factors with opposite effects on flame length as I_{sd} is increased.

The relations:

$$G'_g(x) = \int_0^{R_d} \rho u C'_r dr = \text{const}, \quad M(x) = \int_0^{R_d} \rho u r dr = \text{const}$$

are valid for constant fuel and oxidizing agent delivery rates.

Forced air delivery increases convective transport in the axial portion of the working space, and the velocity is higher; since the reduced fuel flux is constant, the mean integral value of C'_g in the axial region should consequently be lower. On the other hand, turbulent diffusion is reduced with forced air delivery, as a consequence of the smaller transverse velocity gradients, and the transverse C'_g profile, which has a stepped character at the entrace cross section, is therefore deformed less rapidly. The values of C'_g can consequently be higher at the axis than with free air delivery, a pattern manifested in the near-nozzle portion of the flame (Fig. 1).

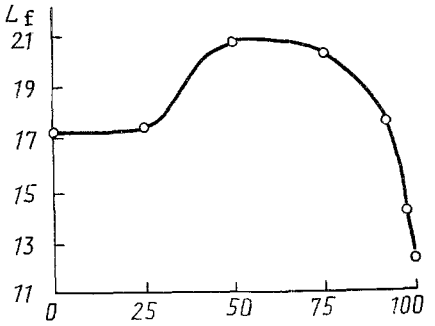

Fig. 3

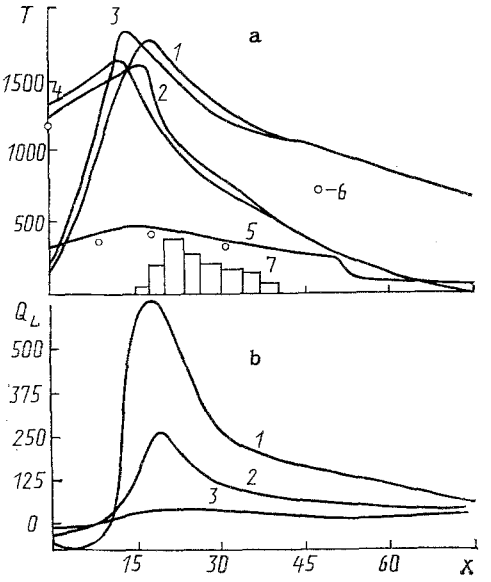

Fig. 4

Fig. 3. Flame length (m) as function of fraction of fuel gas delivered through annular passage (%).

Fig. 4. Results yielded by heat transfer calculations: a) temperature distribution, °C: 1) gas (long flame); 2) material (long flame); 3) gas (short flame); 4) material (short flame); 5) jacket temperature; 6) measured jacket and material temperatures at furnace exit; 7) relative mass of decomposed carbonates; b) linear density of resultant heat flux to material, kW/m: 1) total; 2) at contact boundary with linear; 3) resulting from convective heat transfer.

Flame length is regulated with two-passage burners [2], in which the fuel gas stream can be redistributed between the central nozzles and those in the annulus. We made calculations for flames from a two-passage burner with equal cross-sectional areas for the central and annulus nozzles as the proportion of gas delivered through the annular probability was varied from 0 to 100% while holding total fuel delivery rate constant. Fuel depletion was most rapid when 100% of the gas was delivered through the annular passage, as a consequence of the fact that the contact surface between the fuel and oxidizing agent was greater than for central delivery but maximum initial gas velocity was the same. Flame length was 12 m ($240d_0$), i.e., 65% of the length when all the gas was delivered through the central passage The greatest length was attained with a 50/50 fuel division between the passages. Burner operation approximated to that of a single-passage burner with a nozzle having twice the area of the burner in our case.

Figure 2 shows the temperature at the flame axis, the fuel depletion, and the flame configuration for these extreme cases. The dependence of flame length on the proportion of the fuel delivered through the annular passage is depicted in Fig. 3.

Calculation of furnace gas dynamics in terms of natural variables was employed to determine the pressure loss in the cooler–furnace system, which depends on the degree of furnace wall incrustation, losses to friction, the depth of the material in the feed hopper, and the deflection of the air stream and the simultaneous change in its cross section at the junction of the cooler and furnace. Calculations made with the formulas from [1] lead to significant errors, and we therefore utilized the flame modeling results.

The air stream boundary conditions are not fixed but are calculated with the Bernoulli formula:

$$u_j = \sqrt{\frac{2(\Delta P_j + P_a)}{\rho_0} \frac{T_{ox}}{T_0}},$$

in each iteration, where u_j is the air velocity at a given point in the furnace entrance section, ΔP_j is the pressure drop at this point, and ρ_0 and T_0 are the air density and temperature under standard conditions.

The pressure loss in the air duct is determined by the expression

$$P_a = -(P_r + P_g) + \xi \frac{\rho_{ox} u_{ox}^2}{2}. \quad (8)$$

Th results of calculations made with different flow velocities and pressure losses were given in a previous paper [12]. The air delivery coefficient of 1.1 determined from the experimental data is attained with a pressure loss of 8.0 Pa. The resultant data and the measured pressure drop are employed to determine ξ from Eq. (8) (ξ = 124.2). The value of ξ should be used to determine the pressure loss for a different fuel delivery rate or when the burner is replaced.

Our mathematical model of the complex heat transfer in a rotating furnace is based on a zonal computation procedure, distinguishing the liner, material bed, and gas zones in each section along the length of the furnace. The flame calculations give us the input data: the fuel depletion and gas volume element emissivity for the furnace sections, which are obtained by integrating the concentration within each section over the finite difference net. The mean integral gas stream temperatures over the sections are utilized as the initial approximation.

It has been shown that radiative heat transfer can be adequately taken into account only within the specific section under consideration and the two adjoining it (the triad model) [13]. The bed temperature is assumed to be constant over any cross section, and the rates of the endothermal material decomposition reactions and of evaporation are determined by the resultant heat input to the material.

The nonlinear system of heat balance equations for the individual zones is solved for temperature by Newton's method, recalculating the matrix coefficients in each iteration.

We investigated the influence of flame characteristics on material heating, utilizing the data obtained in flame calculations for an adjustable burner. The material treated was refractory dolomite containing decomposed carbonate. Figure 4 shows the calculated heat fluxes and temperature distributions for the gas, material bed, and liner along the furnace for flame lengths of 20 and 12 m.

Conclusions. The model of an axially symmetric turbulent diffusion flame has been shown to be suitable for investigating the operation of gas-fired RFs. The influence of flame configuration on the temperature distribution in an RF has been investigated.

SYMBOLS

X, axial coordinate; r, radial coordinate; u, axial velocity component; v, radial velocity component; K, kinetic energy of turbulence; ε, rate at which kinetic energy of turbulence is dissipated; C_g', reduced fuel concentration; g, mean square concentration fluctuations; S_F, algebraic (source) term; Γ_F, tubulent transport coefficient; P, pressure; Pr_F, turbulent Prandtl number; μ, molecular viscosity; C_μ, coefficient in turbulent viscosity model; C_g, C_{ox}, C_{or}, fuel, oxidizing agent, and combustion product concentrations; Ω, stoichiometric number; C, average heat capacity from 273 K to T; T_g, T_{ox}, initial fuel and oxidizing agent temperatures; T_f, theoretical combustion front temperature; C_{CO_2}, C_{H_2O}, CO_2 and H_2O concentrations in combustion products in absence of dissociation; α_{CO_2}, α_{H_2O}, degrees of CO_2 and H_2O dissociation; K_1, K_2, equilibrium constants of dissociation reactions; Q_i^f, heat of fuel combustion; $Q^d_{CO_2}$, $Q^d_{H_2O}$, thermal effects of dissociation reactions; q(C), probability density; δ, Dirac function; R_s, radius of furnace working space; I_{sd}, momentum flux densities for oxidizing agent and fuel; ρ, density; $C_g'(x)$, reduced fuel mass flux; M(x), mixture mass flux; P_a, pressure loss in air duct; P_p, pressure loss in furnace entrance section; P_g, geometric pressure; ξ, pressure loss coefficient for cooler–furnace system.

LITERATURE CITED

1. V. A. Krivandin, V. A. Arutyunov, B. S. Mastryukov, et al., Metallurgical Heat Engineering [in Russian], Moscow (1968).

2. I. P. Tsibin, M. Z. Shvartsman, and V. V. Strekotin, Startup, Adjustment, and Heat Engineering Tests for Ovens and Dryers in Refractories Industry [in Russian], Moscow (1978).
3. R. Sullivan and R. Sutton, AIAA Papers, No. 1, 265 (1983).
4. B. Jenkins and F. Moles, Transaction Institution of Chemical Engineers, 200-210 (1981).
5. B. Launder and D. Spalding, Comp. Meth. Appl. Mech. Eng., 3, No. 2, 269-289 (1979).
6. A. D. Gosmen, V. M. Pan, A. K. Ranchil, et al., Numerical Methods for Investigating Flow of Viscous Liquid [in Russian], Moscow (1972).
7. V. V. Bukhmirov, "Improvement of thermal operation of rotating furnace through mathematical modeling of gas dynamics and complex heat transfer," Dissertation, Moscow (1983).
8. D. Spalding, Chem. Eng. Sci., 26, 95-107 (1971).
9. C. Chieng and B. Launder, Numerical Heat Transfer, 3, No. 2, 182-207 (1980).
10. P. Patankar, Numerical Methods for Solving Problems in Heat Transfer and Fluid Dynamics [Russian translation], Moscow (1984).
11. Chan Tam Ngan, "Experimental and theoretical investigation of gas flame in confined space," Dissertation [in Russian], Moscow (1971).
12. V. A. Arutyunov and A. V. Povitskii, Izv. Vyssh. Uchebn. Zaved., Chern. Metallurg., No. 11, 107-109 (1987).
13. V. A. Arutyunov and A. V. Povitskii, Izv. Vyssh. Uchebn. Zaved., Chern. Metallurg., No. 7, 156-157 (1986).

TEMPERATURE DISTRIBUTION IN ZONE SURROUNDING WELL HOLE BOTTOM DURING THERMOCHEMICAL TREATMENT

G. A. Gamidov, V. I. Mamedkerimov, I. A. Nasrullaev, and T. I. Salimov

UDC 622.276.038:522.5

The temperature distribution in the hole bottom zone of a formation during thermochemical treatment is analyzed, taking into account the heat losses through the formation roof and floor. The characteristic parameters of the temperature propagation zones are determined.

Thermochemical methods for acting upon formations are most effective for removing heavy hydrocarbon components from the hole bottom zone and increasing the inflow of crude (particularly high-viscosity crude) to wells [1-6].

The thermochemical treatment that will be considered here involves the exothermal reaction of magnesium with an acid and is carried out by two technological methods: conduct of the reaction in a special chamber at the hole bottom and directly in the formation itself. The first technique entails round-trip operations and possible damage to the lower portion of the string as a result of extensive acid corrosion and is therefore ineffective in comparison with the methods proposed in [7, 8]. These papers described experimental studies of intraformation thermochemical treatment that resulted in transport of the heat source directly into the formation. A solution of starch-based powdered or granulated magnesium was pumped into the formation, followed by a hydrochloric acid solution.

When magnesium mixes with an acid in the percolation zone of a formation, there is an exothermal reaction that liberates a large amount of heat (approximately 4200 kcal of heat is released in the combustion of 1 kg of magnesium, and the temperature is raised to 200-250°C, depending on the magnesium concentration), and the surrounding material is heated. This removes waxes, asphalts, and tars from the hole bottom zone and substantially improves formation conductivity (laboratory studies have shown that permeability increases by a factor of 1.5-2.0 after thermochemical treatment), which leads to a rise in well production rate.

Azerbaidzhan State Scientific-Research and Planning Institute of the Petroleum Industry, Baku. Translated from Inzhenerno-fizicheskii Zhurnal, Vol. 61, No. 3, pp. 414-421, September, 1991. Original article submitted October 26, 1990.